Pharm Res (2021) 38:243–255
https://doi.org/10.1007/s11095-021-02987-0

RESEARCH PAPER

Energetic Dissection of Mab-Specific Reversible Self-Association Reveals Unique Thermodynamic Signatures

Mandi M. Hopkins[1,2] • Arun Parupudi[3] • Jared S. Bee[3,4] • David L. Bain[1]

Received: 11 October 2020 / Accepted: 5 January 2021 / Published online: 18 February 2021

ABSTRACT

Purpose Reversible self-association (RSA) remains a challenge in the development of therapeutic monoclonal antibodies (mAbs). We recently analyzed the energetics of RSA for five IgG mAbs (designated as A-E) under matched conditions and using orthogonal methods. Here we examine the thermodynamics of RSA for two of the mAbs that showed the strongest evidence of RSA (mAbs C and E) to identify underlying mechanisms.

Methods Concentration-dependent dynamic light scattering and sedimentation velocity (SV) studies were carried out for each mAb over a range of temperatures. Because self-association was weak, the SV data were globally analyzed via direct boundary fitting to identify best-fit models, accurately determine interaction energetics, and account for the confounding effects of thermodynamic and hydrodynamic nonideality.

Results mAb C undergoes isodesmic self-association at all temperatures examined, with the energetics indicative of an enthalpically-driven reaction offset by a significant entropic penalty. By contrast, mAb E undergoes monomer-dimer self-association, with the reaction being entropically-driven and comprised of only a small enthalpic contribution.

Conclusions Classical interpretations implicate van der Waals interactions and H-bond formation for mAb C RSA, and electrostatic interactions for mAb E. However, noting that RSA is likely coupled to additional equilibria, we also discuss the limitations of such interpretations.

KEY WORDS analytical ultracentrifugation · dynamic light scattering · interacting systems · monoclonal antibody · nonideality · sedimentation velocity

ABBREVIATIONS

AUC	analytical ultracentrifugation
DLS	dynamic light scattering
mAb	monoclonal antibody;
PBS	phosphate buffered saline
RMSD	root-mean-square deviation
RSA	reversible self-association
SV	sedimentation velocity

The large size and high dosage requirements of therapeutic monoclonal antibodies (mAbs) make them susceptible to multiple forms of degradation (1). Potential sources include conformational instability, colloidal instability, and/or chemical instability (2,3). Such instabilities can lead to formation of irreversible oligomers or aggregates, which may result in injection-site reactivity and immunogenicity (4). Another concern – particularly with regard to practical manufacturing and analytics – is reversible self-association (RSA), defined here as the dynamic exchange of monomers with native-state oligomers. Negative consequences of RSA can include high viscosity of the mAb drug product, long-term conversion to "traditional" irreversible aggregates, phase separation, and opalescence (5–8). Approaches have been proposed to mitigate RSA, including modulation of buffer pH, salt

✉ David L. Bain
david.bain@cuanschutz.edu

[1] Department of Pharmaceutical Sciences, University of Colorado Anschutz Medical Campus, Aurora, Colorado 80045, USA

[2] Present address: Formulation Development, Regeneron Pharmaceuticals, Tarrytown, New York 10591, USA

[3] Department of Dosage Form Design and Development, Biopharmaceuticals R&D, AstraZeneca, Gaithersburg, Maryland 20878, USA

[4] Present address: Formulation and Drug Product Development, REGENXBIO Inc, Rockville, Maryland 20850, USA

concentration, and addition of hydrophobic amino acids (9–11). Additional work has focused on identification of potential interacting residues and regions using homology modeling, followed by mutagenesis and functional analyses (12). Making these findings practicable will require determining the role of buffer formulation on long-term stability and degradation, as well as experimental confirmation of oligomeric structures and their binding interfaces. Noting that it is still the case that a mechanistic understanding of RSA remains incomplete, increased biophysical insight should prove useful in future sequence engineering, redesign of formulation conditions to modulate self-association properties, and provide additional context to potential clinical impacts of RSA.

We previously carried out an analysis of the energetics of RSA for five IgG mAbs (designated here as A-E) under matched conditions and using orthogonal methods (13). Using concentration-dependent dynamic light scattering (DLS) and sedimentation velocity (SV), we found that the majority of mAbs examined exhibited some degree of RSA. However, because the interaction affinities were weak, we also observed significant thermodynamic and hydrodynamic nonideality. As noted above, we define RSA as the dynamic exchange of monomers with higher-order oligomers, whereas thermodynamic nonideality, BM_1, reflects contributions from macromolecular charge and excluded volume (14). Hydrodynamic nonideality is less precisely defined, but also includes contributions from charge and volume (15). For self-associating systems, formation of oligomers will result in a concentration-dependent increase in the weight-average sedimentation coefficient and broadening of the sedimentation coefficient distribution. However, at high concentrations, hydrodynamic nonideality generates a concentration-dependent slowing and sharpening of the distribution, while thermodynamic nonideality leads to slight spreading of the distribution (16). Thus for weakly interacting systems, self-association and nonideality mask the presence of each other and therefore confound the ability to extract interaction parameters such as K_{eq}, K_s and BM_1. A detailed analysis of the challenges in interpreting and analyzing such systems was recently published by Correia and coworkers (17). To address these issues, we carried out direct boundary fitting for each of the five mAbs. This approach revealed a variety of mAb-specific RSA behavior, including differences in interaction affinity, kinetics, and type of self-association model (e.g. monomer-dimer *versus* monomer-dimer-tetramer). The accuracy of the models and their corresponding interaction terms were further examined using sedimentation equilibrium, with the collective results forming the basis for future studies of the underlying molecular forces responsible for mAb-specific RSA.

Here we examine the thermodynamics of RSA using two of the mAbs that showed the highest propensities for self-association, mAb C and E. Following the approach described above, we determined the energetics of RSA over a range of temperatures (10to 35°C) to estimate underlying enthalpic and entropic terms. Dynamic light scattering and sedimentation velocity (SV) approaches were again used, with the SV data analyzed by direct boundary fitting. For mAb C, model testing indicated that the antibody undergoes isodesmic or indefinite self-association at all temperatures examined, with the temperature-dependent affinities indicative of a strong enthalpic contribution offset by a significant entropic penalty. By contrast, mAb E undergoes monomer-dimer self-association at all temperatures, with the reaction being primarily entropically-driven and comprising only a small enthalpy contribution. Although interpretation of the enthalpy and entropy values is not straightforward, the unique thermodynamic signatures for each mAb suggest that distinct mechanisms underlie their self-association. Moreover, because self-association for both mAbs is likely coupled to multiple equilibria – including proton, ion-binding and water release reactions – the thermodynamic parameters determined here presumably represent a composite of many molecular contributions. Potential interpretations are discussed.

MATERIALS AND METHODS

Reagents

Highly purified mAbs C and E (subclass IgG1) were provided by MedImmune LLC (now a member of AstraZeneca). Both mAbs have been previously reported to undergo RSA, and have served as prototypes for understanding the underlying mechanisms (10,12,13,18–22). Each mAb was dialyzed from stock concentration into phosphate buffered saline (PBS) at pH 7.4 (137 mM NaCl, 2.7 mM KCl, 10mM Na_2HPO_4, 1.8 mM KH_2PO_4). Final protein concentrations were determined by absorption spectroscopy ($A_{280\ nm}$) using an extinction coefficient provided by MedImmune (1.56 mL mg^{-1} cm^{-1} for both mAbs). A calculated partial specific volume of 0.7245 mL/g, weighted for 2% glycan mass, was also used. The buffer density and viscosity at 10, 15, 20, 25, 30, and 35°C were determined using the public domain software program SEDNTERP (www.jphjilo.maiway.com) (23).

Dynamic Light Scattering

The concentration-dependent, hydrodynamic diameter (D_H) for each mAb was determined at 4, 20 and 37°C using a Zetasizer Nano ZSP DLS instrument (Malvern), equipped with a 633 nm He-Ne laser. Scattered light was monitored at 173° to the incident beam. 120 µL of sample were loaded into the quartz cuvette covering a concentration range of 1 to 15 mg/mL for mAb C and 1 to 20 mg/mL for mAb E. Data were collected using 120 s of equilibration time, followed by three 10-s acquisitions per sample. The hydrodynamic

diameter and mutual diffusion coefficient at each concentration were calculated via fitting of the autocorrelation function using algorithms incorporated in the Malvern software. Prior to dilution and analysis, samples were buffer-exchanged using Amicon Ultra-0.5 centrifugal filters and filtered with Durapore 0.22 μm PVDF membrane filters. Temperature-dependent solution viscosities were determined using an Anton Paar Lovis 2000 M/ME microviscometer.

Sedimentation Velocity Analytical Ultracentrifugation

SV experiments were carried out at 10, 15, 20, 25, 30 and 35°C using a Beckman XLI analytical ultracentrifuge (Beckman Coulter) equipped with interference optics and an An-50 Ti rotor. Samples in concentrations ranging from 0.3 to 10 mg/mL for mAb C and 0.3 to 13 mg/mL for mAb E were loaded into two-sector 3 or 12 mm Epon centerpieces with sapphire windows. The 3 mm centerpieces were used for all mAb concentrations greater than 1 mg/mL. Samples were allowed to reach temperature equilibrium for at least 1 h (overnight for the more extreme temperatures) before centrifugation at 42,000 rpm. Data were collected by interferometry every 60 s until samples were completely pelleted, and analyzed for sedimentation distributions using DCDT+, version 2.4.3 (24,25). Global boundary fitting and statistical analyses were carried out using SEDANAL, version 7.17 (http://www.sedanal.org) (26). When preprocessing the data, scans collected later in each sedimentation run (50 to 100 scans per mAb concentration) were chosen for global analysis.

As explained in more detail elsewhere (26), data were fit to an expansion of the numerical solution to the fundamental Lamm equation (Eq. 1) by finite-element analysis using the method of Claverie (27,28).

$$\left(\frac{\partial c}{\partial t}\right)_r = 2\frac{\partial}{\partial \xi}\left[D\xi\left(\frac{\partial c}{\partial \xi}\right)_t - \omega^2 sc\xi\right] \tag{1}$$

where c is the concentration as a function of t and ξ, $\xi = r^2/2$, t is time, D is the diffusion coefficient and s is the sedimentation coefficient. The concentration dependence of the sedimentation coefficient, $s(c)$, and the diffusion coefficient, $D(c)$, were incorporated via Eqs. 2 and 3,

$$s(c) = \frac{S_0}{(1 + k_s c)} \tag{2}$$

$$D(c) = \frac{D_0(1 + 2BM_1 c)}{1 + k_s c} \tag{3}$$

where K_s is the hydrodynamic nonideality, thermodynamic nonideality is represented through the second virial coefficient, BM_1, and s_0 and D_0 are the sedimentation and diffusion coefficients at infinite dilution, respectively.

The model editor in SEDANAL allows for creation and editing of any model ranging from single species to various combinations of non-interacting and interacting species (e.g. monomer-dimer, isodesmic) and their associated reaction schemes. For the mAbs examined here, SEDANAL will globally fit the data to the expansion of the Lamm equation for multiple species (Eq. 4),

$$\left(\frac{\partial c}{\partial t}\right)_r = \sum_{i=1}^{N}\left(\frac{\partial c_i}{\partial t}\right)_r = 2\sum_{i=1}^{N}\frac{\partial}{\partial \xi}\left[D_i\xi\left(\frac{\partial c_i}{\partial \xi}\right)_t - \omega^2 s_i c_i \xi\right] \tag{4}$$

where N is the number of species. For reacting systems such as monomer-dimer or isodesmic, the model editor also includes the relevant binding constants using the monomer concentration as a reference. Finally, 95% confidence intervals on the fitted parameters were determined by F-statistics, and cross-correlation analyses were determined using bootstrap with replacement approaches, both as implemented in SEDANAL.

RESULTS

DLS Studies Reveal that mAbs C and E Display Different Temperature Dependencies of RSA

To assess how temperature influences the self-association of each mAb, we first carried out DLS studies. Shown in Fig. 1a are concentration-dependent hydrodynamic diameters for mAb C determined at 4, 20 and 37°C. At all temperatures, the hydrodynamic diameter, D_H, increases with concentration, thus indicative of self-association. However, RSA is also highly temperature-dependent, being most prominent at 4°C and decreasing significantly as temperature is increased. We also note some curvature in the concentration-dependent change in diameter, especially at 4°C. This likely reflects the high affinity formation of mAb C oligomers leading to a steep increase in diameter at low concentrations, followed by solution nonideality increasingly suppressing the apparent diameter at higher concentrations (29).

Shown in Fig. 1b are the same results now determined for mAb E. Although mAb E also displays an increase in hydrodynamic diameter consistent with RSA, the extent of self-association appears to be weaker than mAb C based on the smaller change in diameter. Also distinct from mAb C, there is little evidence of any temperature dependence. Consistent with the above interpretations, the k_d values for both mAbs are negative and thus indicative of attractive interactions, with mAb C again showing a temperature dependence whereas mAb E does not (Table I). A representative plot of the mutual diffusion coefficients as a function of mAb E concentration is shown in Fig. 1c.

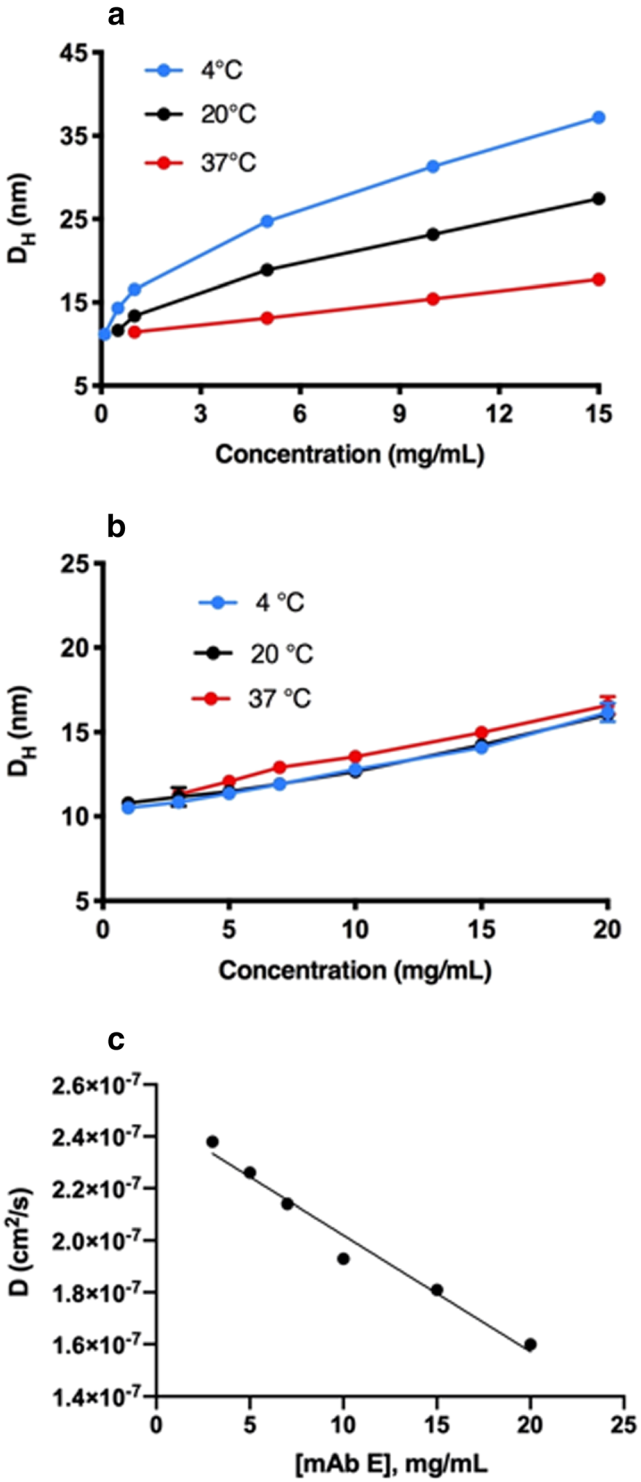

Fig. 1 Concentration-dependent DLS results for mAbs C and E as a function of temperature. Data were collected at concentrations covering 0.5 to 15 mg/mL for mAb C (panel **a**), and 1 to 20 mg/mL for mAb E (panel **b**). Studies were carried out in PBS and temperatures of 4°C (blue), 20°C (black) and 37°C (red). A representative plot of the mutual diffusion coefficient as a function of mAb E concentration (4°C) is shown in panel C. Error bars represent SD from at least three independent experiments.

Table I Estimated k_d Values as a Function of Temperature as Determined by DLS

Temperature (°C)	mAb C k_d (ml/g)	mAb E k_d (mL/g)
4	−49.2 ± 13.1	−18.1 ± 1.5
20	−38.7 ± 7.4	−17.2 ± 1.6
37	−27.2 ± 2.6	−18.5 ± 1.2

Sedimentation Velocity Studies Reveal Extensive Self-Association for mAb C, Less so for mAb E

To probe the energetics of mAb C and E RSA along with the underlying thermodynamic contributions, we carried out SV studies as a function of temperature. The buffer conditions were identical to the DLS studies and covered a wide range of temperatures (10 to 35°C). The data were first analyzed in a model-independent fashion using *g(s*)* analysis to assess the extent of RSA, potential contributions from nonideality, and the presence of irreversibly-formed species.

Shown in Fig. 2a are representative *g(s*)* distributions for mAb C at 10, 20 and 35°C. As seen at 10 and 20°C especially, mAb C generates a broad distribution in *S* values that right-shifts with increasing concentration. The wide and smooth distribution at all concentrations suggests the presence of multiple oligomeric states in rapid equilibrium. Hydrodynamic nonideality is observed as peak sharpening and a slight left-shift of the distribution at the highest concentrations. Evidence of irreversibly-formed species are seen as a concentration-independent shoulder at 9–10 *S*, which is most obvious at the low concentration distributions at 35°C. Based on their sedimentation coefficients, these latter species likely represent irreversible dimer (13). Finally, we also observe a strong decrease in RSA with increasing temperature, consistent with the DLS results.

Shown in Fig. 2b are the analogous *g(s*)* distributions for mAb E. The distributions show only modest sensitivity to increasing mAb concentration, consistent with the DLS results and suggestive of a weak self-association reaction. Additionally, the concentration-independent shoulder at 9–10 *S* again suggests the presence of irreversibly-formed dimer. Although nonideality is not visually present as it was for mAb C, based on our previous studies this is due to the weak self-association masking hydrodynamic nonideality. Finally, the distributions show little temperature dependence, similar to the DLS results.

Direct Boundary Fitting: mAb C Undergoes Temperature-dependent, nonideal isodesmic self-association

To determine self-association models, interaction affinities, and nonideality terms for both mAbs and at all temperatures,

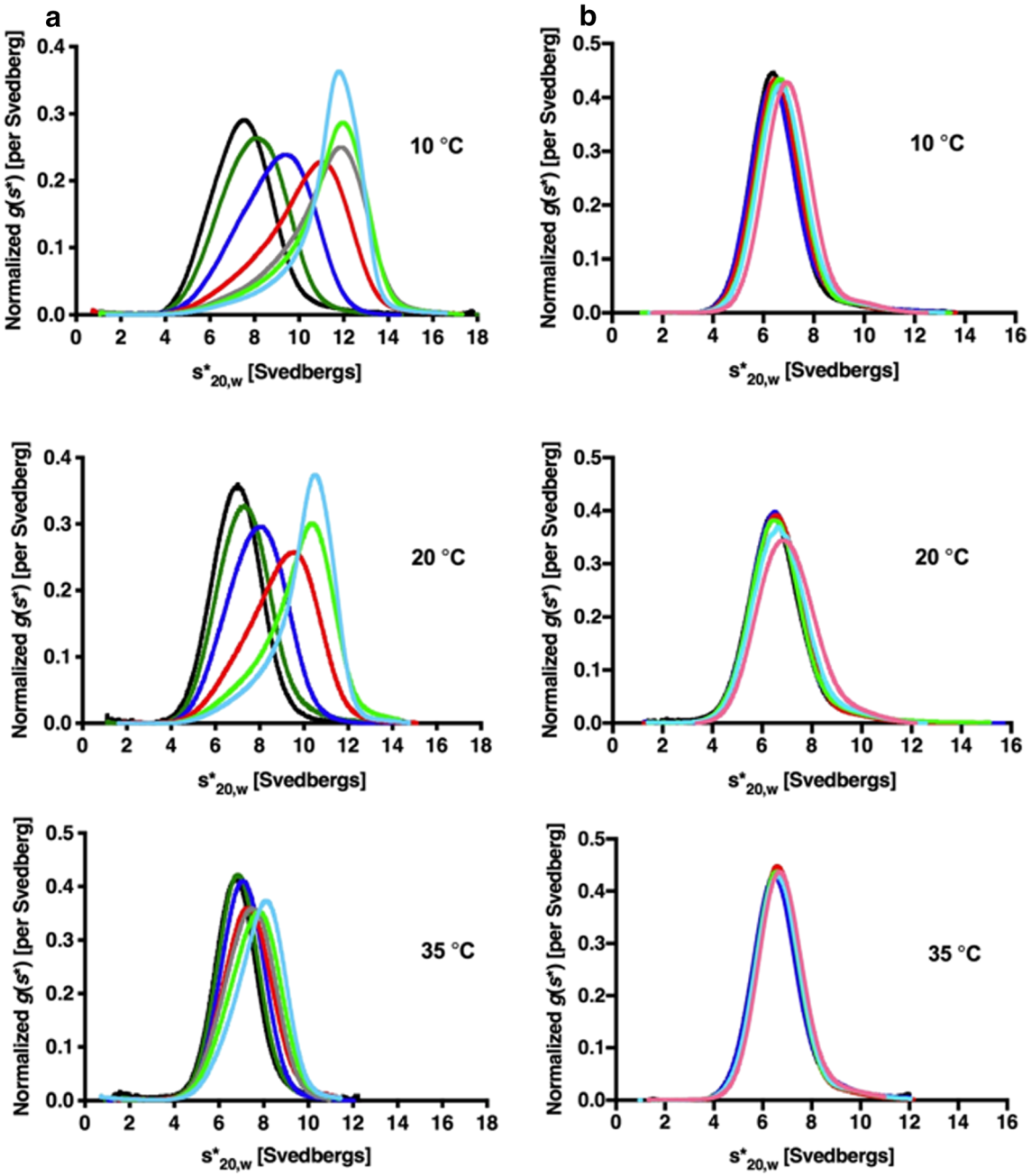

Fig. 2 Concentration-dependent *g(s*)* analysis for mAbs C and E as a function of temperature. a Representative *g*(*s**) profiles of mAb C at 0.3 (black), 0.5 (green), 1 (blue), 3 (red), 5 (grey), 7 (light green), and 10 (light blue) mg/mL in PBS, and at 10, 20 and 35°C. **b** Representative *g*(*s**) profiles of mAb E at 0.3 (black), 1 (blue), 3 (red), 7 (light green), 10 (light blue), and 13 (pink) mg/mL in PBS, and at 10, 20 and 35°C.

we carried out direct boundary fitting. For mAb C specifically, concentrations ranging from 0.3 to 10 mg/mL were globally fit to a wide variety of models, with initial model choices guided by our previously published results and assessment of the model-independent *g(s*)* plots in Fig. 2a. For each model, we locked parameters for which we had independent knowledge (e.g. mAb molecular weight), and constrained the relationship among sedimentation coefficients regardless of whether those parameters were locked or unlocked. As an example of the latter, for simple models such as monomer-dimer we constrained respective sedimentation coefficients based on estimating their *S* values from fitting a low-concentration data set where no RSA was occurring, but irreversibly-formed dimer was present (e.g. 0.3 mg/mL at 35°C). For more complicated models (e.g. isodesmic) in which it was not possible to infer structural information on all higher-order oligomers, we

constrained *S* values using the $s_n = s_1 n^{2/3}$ rule, where n refers to stoichiometry and s_1 is the monomer s value (30). Alternative expressions for relating the monomer s value to those of the higher-order species [see Ref. 31 for example] influenced the estimated sedimentation coefficients, but had no significant impact on the interaction affinities.

Upon global fitting, parameters were successively unlocked ("floated") to assess their contribution to the overall fit. Key parameters of interest were the sedimentation coefficient of the monomer (s_1); the association constant(s) for RSA (K_{eq}); hydrodynamic nonideality (K_s); thermodynamic nonideality (BM_1); and the proportion of irreversible dimer. With the exception of the 35°C data, the results we report for mAb C were determined when all of the above parameters were simultaneously floated in the global fit. This approach follows the strategy of Correia and Stafford for estimating interaction parameters from SV data in SEDANAL (32). Analysis of simulated data also proved useful for assessing our ability to discriminate among models and reliably estimate interaction parameters (not shown).

With regard to mAb C, we previously found that self-association in PBS at 20°C was best described by an isodesmic reaction scheme ($A + A \Leftrightarrow A_2$; $A + A_2 \Leftrightarrow A_3$; $A + A_3 \Leftrightarrow A_4$;…) (13). To determine if this model was most appropriate for the temperatures examined here, we again tested a variety of reaction schemes, a subset of which are summarized in Table II. Here we use the mAb C SV data collected at 10°C as a testcase since it showed the greatest extent of self-association (Fig. 2a, top panel). Shown in Fig. 3 is a global fit of the 10°C data to a nonideal isodesmic model. The isodesmic model well-describes all datasets, having an RMSD of 0.023 fringes. As summarized in Table III, the fit returned an $s_{20,w}$ for the monomer of 6.78 *S*, a K_{eq} of 5.92e4 M^{-1}, a K_s of 29.6 ml/g and a BM1 of 17.4 ml/g. (This fit and all others also included a term to account for irreversibly-formed dimer, typically about 2% and not reported here.) Although the sedimentation coefficient and affinity term were generally consistent with expectations, the nonideality terms were not – theory and experiment suggest K_s and BM_1 should be in the range of 2–11 mL/g for a mAb monomer (14,15,33–35). We had observed this previously and address the interpretation later in the Discussion (13).

Noting that mAb C self-association has been described by alternative reaction schemes, albeit under conditions different from those used here (10,18), we also tested a variety of additional models. These included monomer-dimer-tetramer, monomer-trimer-hexamer, Adair models (i.e. models that allow for sequential binding of a single protomer to a discrete end-state), and concerted reactions such as monomer-hexamer. Additionally, because mAbs are capable of forming hexameric rings under certain conditions (e.g. in the presence of complement) (36) we also tested closed reaction schemes.

In general, we found that all non-consecutive self-association schemes – that is, reactions in which more than one protomer at a time is added to the growing oligomer – resulted in poor fits with visually obvious systematic residuals. For example, fitting the data to a monomer-trimer-hexamer model returned an RMSD of 0.087 fringes or roughly four-fold worse than the isodesmic fit. Concerted reactions and ring-closure reactions also resulted in poor fits. By contrast, fitting the data to Adair-type self-association reactions (e.g. monomer-dimer-trimer-tetramer-pentamer) resolved similar interaction affinities as the isodesmic model and best approached the quality of fit of the isodesmic model once sufficient higher-order species were included. For example, an Adair model including species out to tetramer returned an RMSD of 0.069 fringes, whereas once species out to pentamers or hexamers were added, the RMSDs decreased to 0.052 and 0.036 fringes, respectively. Adair models that included species of heptamer or greater offered no improvement of the fit relative to the hexamer model. Representative models used for analysis and their best-fit RMSDs are shown in Table II.

Table II Representative Models and Best-Fit RMSDs for mAb C SV Data Collected at 10 °C

Model	RMSD (fringes)
Monomer-hexamer (i.e. concerted)	~0.5 (failed to converge)
Closed hexamer	~0.2 (failed to converge)
Monomer-dimer-tetramer	~0.2 (failed to converge)
Monomer-trimer-hexamer	0.087
Monomer-dimer-trimer-tetramer	0.069
Monomer-dimer-trimer-tetramer-pentamer	0.052
Monomer-dimer-tetramer-hexamer	0.039
Monomer-dimer-trimer-tetramer-pentamer-hexamer	0.036
Isodesmic	0.023

With the exception of the monomer-hexamer model, all interaction affinities were fit as sequential equilibria constants in order to best compare to the sequential affinity estimated in the isodesmic model

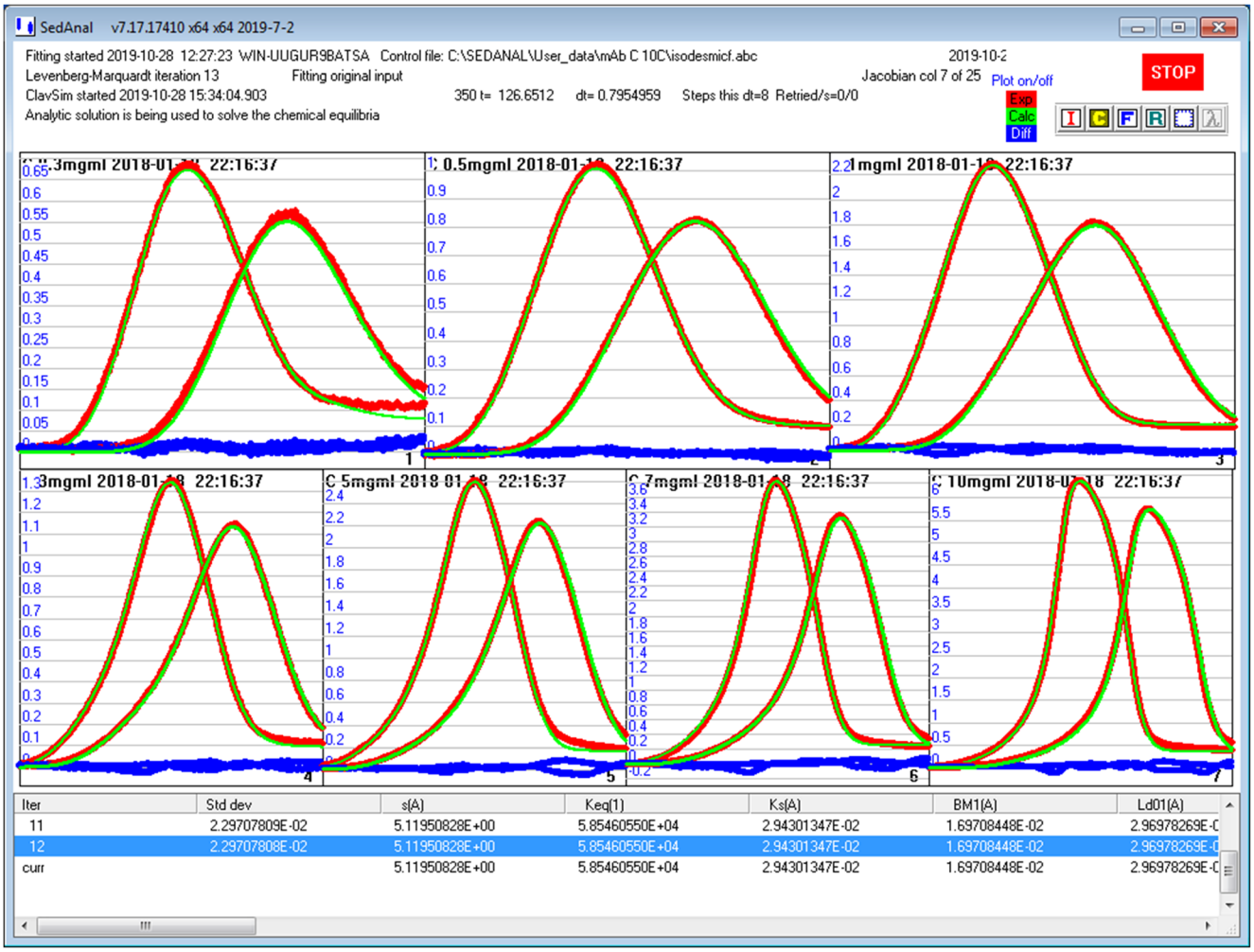

Fig. 3 Global analysis of mAb C SV data to a nonideal, isodesmic self-association model. Scans were collected at 10°C in PBS, and at 0.3, 0.5, 1, 3, 5, 7 and 10 mg/mL. Data (in red) are shown as difference scans in units of Δfringes *versus* radius. Best fit is shown in green, with residuals shown in blue. 50 to 100 scans were analyzed at each concentration, resulting in 25 to 50 difference scans; only the first and last difference scans at each concentration are shown for clarity. Top row: 0.3, 0.5, and 1 mg/mL mAb C; bottom row: 3, 5, 7 and 10 mg/mL mAb C.

The above approach was repeated for the mAb C data collected at all remaining temperatures, with the isodesmic model consistently resulting in the best fit. The interaction parameters covering the entire temperature range are summarized in Table III. Finally, we note that at the highest temperature of 35°C where the weakest self-association was observed (see Fig. 2a, bottom panel), we were unable to reliably estimate nonideality terms, especially K_s. This is due to strong correlation between K_{eq} and K_s, which results in the underestimation of both parameters (16). For example, attempts to float K_s resulted in a value that approached 0 mL/g and a K_{eq} on the order of 100 M^{-1}. Noting that hydrodynamic nonideality is sufficiently strong to be visually observed in the data (see Fig. 2a), and the estimated K_{eq} term corresponds to a 10 mM dissociation constant when the highest experimental mAb concentration was only 68 μM, these estimates are unrealistic. Based on our previous work and that of others (13,34,35), we therefore locked the nonideality terms, K_s and BM_1, at intermediate values of 6 and 5.4 ml/g, respectively.

Direct Boundary Fitting: mAb E Exhibits Nonideal Monomer-Dimer Self-Association

We previously examined the self-association of mAb E in PBS at 20°C, finding it underwent nonideal monomer-dimer self-association (13). Shown in Fig. 4 is a global fit to the 10°C data using such a model (and incorporating an irreversible dimer term). This model well-describes all data sets, resulting in an RMSD of 0.042 fringes, an $s_{20,w}$ of 6.46 *S* and a K_{eq} of 1.72e3 M^{-1}. Similar to the situation for mAb C at 35°C, the relatively weak K_{eq} value generated strong correlation between parameters, making it necessary to lock K_s and BM_1 at 6 and 5.4 mL/g, respectively. Attempts to fit the data to more complex models (e.g. monomer-dimer-trimer) offered no improvement in fit relative to the monomer-dimer model, whereas fitting to a noninteracting monomer model with or without nonideality resulted in a poor fit with strong systematic residuals (RMSD of ~0.2 fringes). A similar result was seen at all

Table III Estimated Parameters Determined from Direct Boundary Fitting of mAb C SV Data to a Nonideal Isodesmic Model with Irreversible Dimer

Temperature (°C)	$s_{20,w}$	K_{eq} (M^{-1})	K_s (mL/g)	BM_1 (mL/g)	RMSD (fringes)
10	6.78 (6.75, 6.79)	5.92e4 (5.86e4, 6.02e4)	29.6 (29.3, 29.7)	17.4 (16.6, 18.0)	0.023
15	6.53 (6.49, 6.56)	4.72e4 (4.61e4, 4.84e4)	26.7 (26.4, 27.0)	15.2 (14.2, 16.2)	0.025
20	6.42 (6.41, 6.43)	3.37e4 (3.26e4, 3.47e4)	23.6 (23.3, 23.7)	9.4 (9.0, 9.6)	0.022
25	6.43 (6.43, 6.44)	2.26e4 (2.20e4, 2.31e4)	18.6 (18.4, 18.8)	8.5 (8.1, 9.0)	0.021
30	6.46 (7.97. 7.99)	1.35e4 (1.34e4, 1.36e4)	15.2 (15.1, 15.3)	4.8 (4.7, 7.9)	0.025
35	6.43 (6.42, 6.44)	9.21e3 (9.13e3, 9.24e3)	6.0 (locked)	5.4 (locked)	0.018

95% confidence intervals determined by F-statistics as implemented in SEDANAL

other temperatures, and a summary of the estimated K_{eq} and *S* terms is shown in Table IV.

The temperature-dependent association constants for each mAb were used to estimate enthalpy and entropy terms for self-association. As shown in Fig. 5, van't Hoff analysis indicates a strong temperature dependence for mAb C RSA and a near-negligible dependence for mAb E. Linear fits to the data returned a self-association enthalpy of −13.3 ± 1 kcal/mol for mAb C and −1.6 ± 0.8 kcal/mol for mAb E. Using the affinity constants in Tables III and IV, the entropy terms at 20°C (expressed as TΔS) were estimated at −7.2 ± 1 kcal/mol for mAb C and +2.6 ± 0.9 kcal/mol for mAb E.

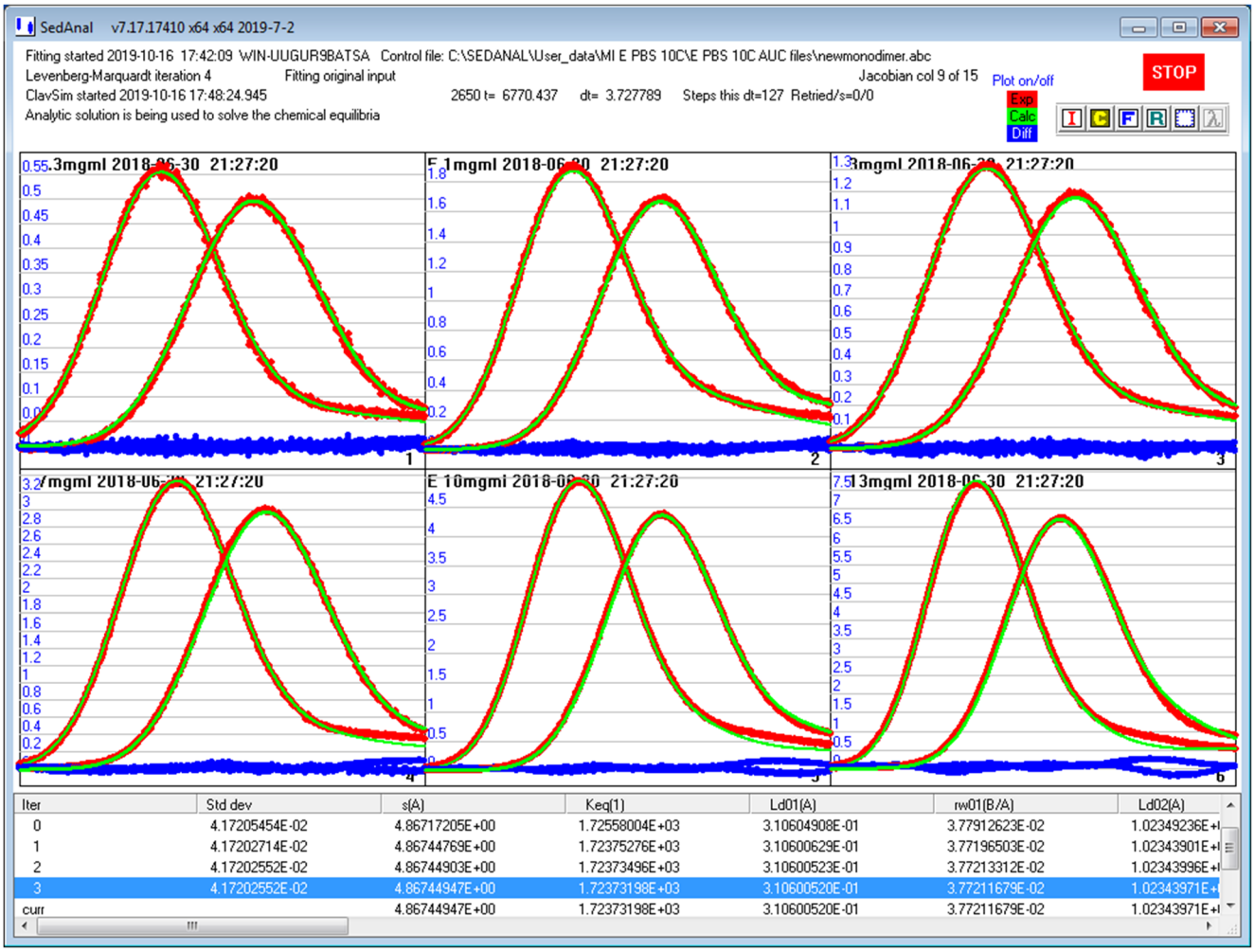

Fig. 4 Global analysis of mAb E SV data to a nonideal, monomer-dimer self-association model. Scans were collected at 10°C in PBS, and at 0.3, 1, 3, 7, 10 and 13 mg/mL using interference optics. Data (in red) are shown as difference scans in units of Δfringes *versus* radius. Best fit is shown in green, with residuals shown in blue. 50 to 100 scans were analyzed at each concentration, resulting in 25 to 50 difference scans; only the first and last difference scans at each concentration are shown for clarity. Top row: 0.3, 1 and 3 mg/mL mAb E; bottom row: 7, 10 and 13 mg/mL mAb E.

Table IV Estimated Parameters Determined from Direct Boundary Fitting of mAb E SV Data to a Nonideal Monomer-Dimer Model with Irreversible Dimer

Temperature (°C)	$s_{20,w}$	K_{eq} (M^{-1})	RMSD (fringes)
10	6.46 (6.44, 6.47)	1.72e3 (1.69e3, 1.78e3)	0.042
15	6.42 (6.41, 6.44)	1.85e3 (1.79e3, 1.91e3)	0.042
20	6.31 (6.30, 6.32)	1.53e3 (1.49e3, 1.59e3)	0.043
25	6.45 (6.44, 6.46)	1.40e3 (1.35e3, 1.45e3)	0.044
30	6.43 (6.41, 6.44)	1.34e3 (1.28e3, 1.40e3)	0.046
35	6.39 (6.38, 6.40)	1.53e3 (1.46e3, 1.56e3)	0.042

95% confidence intervals determined by F-statistics as implemented in SEDANAL

K_s and BM_1 terms were locked at 6 mL/g and 5.4 mL/g, respectively

DISCUSSION

Is mAb C Self-Association Isodesmic?

Due to its propensity to self-associate, mAb C has long served as a prototype for exploring the mechanisms of mAb-specific RSA (10,18). Proposed self-association models include monomer-trimer-hexamer, monomer-trimer-hexamer-nonamer, isodesmic by trimer, and traditional isodesmic. Under the conditions examined here – a subset of which were quite different from those of previous studies, including differences in temperature, pH and ion concentration – self-association was best described using an isodesmic reaction scheme. This conclusion was reached after testing a wide variety of models and analyzing datasets collected over a range of temperatures. Our findings did not change when analyzing only subsets of data; nor did they change when we varied the constraints on sedimentation coefficients beyond the traditional $s_n = s_1 n^{2/3}$ rule via the use of HYDRO++ to model alternative higher-order structures (31,37). Finally, isodesmic self-association as a best-fit model was consistent with our previous analysis of mAb C, which employed both sedimentation equilibrium and sedimentation velocity studies (13).

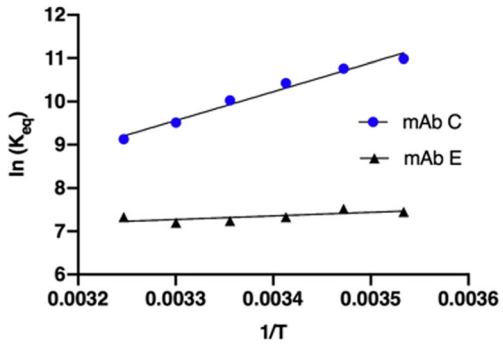

Fig. 5 van't Hoff analysis of the temperature-dependence of mAb C and E self-association. Interaction affinities (K_{eq}) determined from global fitting of the SV data (see Tables I and 2) were plotted in natural log units *versus* inverse temperature to determine enthalpies of self-association. Linear fits to the data returned an enthalpy of −13.3 ± 1 kcal/mol for mAb C and −1.6 ± 0.8 kcal/mol for mAb E. Confidence intervals of affinity terms are too small to be seen in plot. The estimated enthalpy terms were statistically insensitive to fitting only subsets of data points.

We nonetheless feel that the isodesmic model should be seen as provisional for the time-being. Shown in Fig. 6 are the calculated concentrations of mAb C monomer and higher-order oligomers at the three highest protein concentrations examined assuming an isodesmic reaction scheme**.** It is evident that even at the highest concentration of 10 mg/mL, species greater than hexamer are only weakly populated. Consistent with this, fitting of Adair models that included species up to hexamer were the second-best fit to the data (see Table I), and no improvement in the fit was seen upon addition of species beyond hexamer. However, if an isodesmic model is indeed "correct", a prediction of such a model is that an Adair reaction scheme should equally well-describe the data once sufficient higher-order species are included. As seen in Table I, this is clearly not the case, with an Adair model including hexamers or greater being ~50% worse than the isodesmic model. More generally, we found that if we force-fit various models to synthetic data generated from an isodesmic model, we observed only qualitative agreement with the rank-ordering seen in Table I (not shown). These discrepancies suggest that additional factors contribute to the fitting results (e.g. sample microheterogeneity) and/or that mAb C undergoes a more complex self-association reaction than traditional isodesmic.

Currently, we do not have enough information to definitively assign a reaction scheme for mAb C self-association. However, a step in the right direction would be to independently determine the structures of the higher-order oligomers (e.g. via electron microscopy). An added benefit of a structural analysis would be the hydrodynamic modeling of individual oligomeric species, identification of self-association interfaces, and homology modeling of charge distributions and hydrophobic regions, resulting in a more accurate estimate of mAB C sedimentation coefficients, interaction parameters, and additional insight into the forces responsible for self-association. This combined approach has proven highly effective in the analysis of other complex, highly self-associating systems such as β-tubulin and ClpB (31,38). With regard to the gross nature of self-association, it is generally thought that Fab regions contribute, although recent work has also demonstrated a role for the Fc region (19).

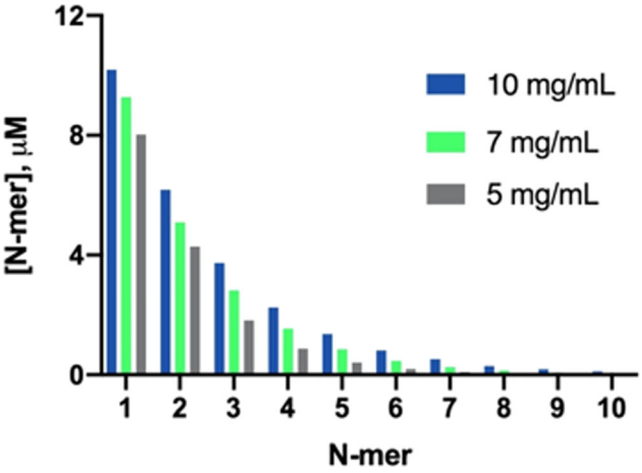

Fig. 6 Predicted concentrations of mAb C monomer and higher-order oligomers (N-mers) assuming an isodesmic self-association model. Interaction parameters determined at 10°C (see Table I) were used to calculate the molar concentration of monomer and higher-order oligomers at three mAb C concentrations using an isodesmic self-association model: 10 mg/mL (blue), 7 mg/mL (green) and 5 mg/mL (blue). Calculations were carried out using SEDANAL.

Finally, we observed unexpectedly large nonideality values for mAb C, particularly for K_s (see Table II). We had observed this previously at a single temperature (13), although the underlying origins were unclear. A general expression for K_s has been derived by Rowe, in which:

$$K_s = 2\overline{v}\left[\frac{V_s}{\overline{v}} + \left(\frac{f}{f_o}\right)^3\right] \quad (5)$$

where $\overline{v}$ is the solute partial specific volume (mL/g), V_s is the solute specific volume (mL/g), and f/f_o is the solute frictional ratio (unitless) (15). Here V_s describes the volume per unit mass occupied by the mAb and any "entrained solvent" (i.e. strongly and weakly-bound solvent molecules). In contrast, f/f_o provides gross structural insight, with values greater than 1 indicative of a deviation from compact sphere. K_s can thus be seen as being made up of a solvation term, $V_s/\overline{v}$, and a shape term, f/f_o. As noted earlier, we currently have little insight into the structure of the mAb C oligomers and so it is not possible to determine their f/f_o values. However, work by Philo demonstrates that at least for irreversibly-formed oligomers out to hexamer, f/f_o is comparable to that of the monomer, staying constant at 1.5 to 1.6 (39). If we assume that those findings hold for the reversibly-formed oligomers analyzed here, then the K_s term for each oligomer is primarily influenced by its stoichiometric increase in V_s. For example, if one assumes a K_s value of 10 mL/g for the mAb C monomer, the K_s values for dimer, trimer, tetramer, pentamer and hexamer can be calculated as 15, 20, 25, 30 and 35 mL/g, respectively.

We note that the K_s values reported in Table II represents an average across all species in solution. (It is not possible to individually fit for each K_s value.) This suggests that at lower temperatures, where the increased affinity of self-association drives the formation of additional oligomers, the large K_s values we observe experimentally reflect contributions from the increased K_s values of dimer, trimer, tetramer, etc. Consistent with this, if we simulate data using the above calculated K_s values for each of these species, and then force-fit the data to a model allowing only single average K_s, the fit returns a value well above that of a monomer (not shown).

Regarding BM_1, it is again the case that it represents an average across all species in solution. Thus, the larger BM_1 values seen at lower temperatures presumably reflect an increased population of oligomers with larger individual BM_1 values. In principle, BM_1 should be identical for all species; however, this is only the case if charge, shape, and hydration remain constant for all species (14). If we again assume that the f/f_o value for all species remains unchanged, this suggests that mAb charge and/or hydration state are being perturbed upon oligomer formation. To our knowledge, it is not generally possible to calculate BM_1 values for the individual species beyond using simple sphere or rod-like shape assumptions (14); nor are we certain that the isodesmic model is truly the "correct" model (e.g there may be multiple oligomer shapes at any given stoichiometry). Thus, considerably more biophysical and structural work will be necessary to shed mechanistic light on the origins of the experimentally observed BM_1 (and K_s) values.

What about mAb E?

Here we find that mAb E undergoes weak monomer-dimer self-association at all temperatures. This is consistent with what we observed previously at 20°C (13), although others have found association to tetramer (19). Noting that the latter studies were carried out at acidic pH and a range of salt concentrations, mAb E RSA is likely coupled to additional proton- and ion-binding reactions. This possibility is discussed in more detail below.

Although the analysis of mAb E was more straightforward than that of mAb C, for both mAbs we were forced to lock the nonideality terms at calculated values when estimating weak affinities. As has been discussed previously (16,17), this is due to the masking effect of K_s on K_{eq} and vice-versa, resulting in strong correlation between the two parameters. This phenomenon can be appreciated visually in Fig. 7. Shown are correlation plots determined by bootstrap simulations using a non-ideal monomer-dimer model and the parameter values determined at 10°C for mAb E (see Table IV). After thirty simulations, key parameters were plotted against each other and the extent of correlation determined by straight-line fits. As shown in Fig. 7a, K_s and K_{eq} are most correlated (R = 0.96),

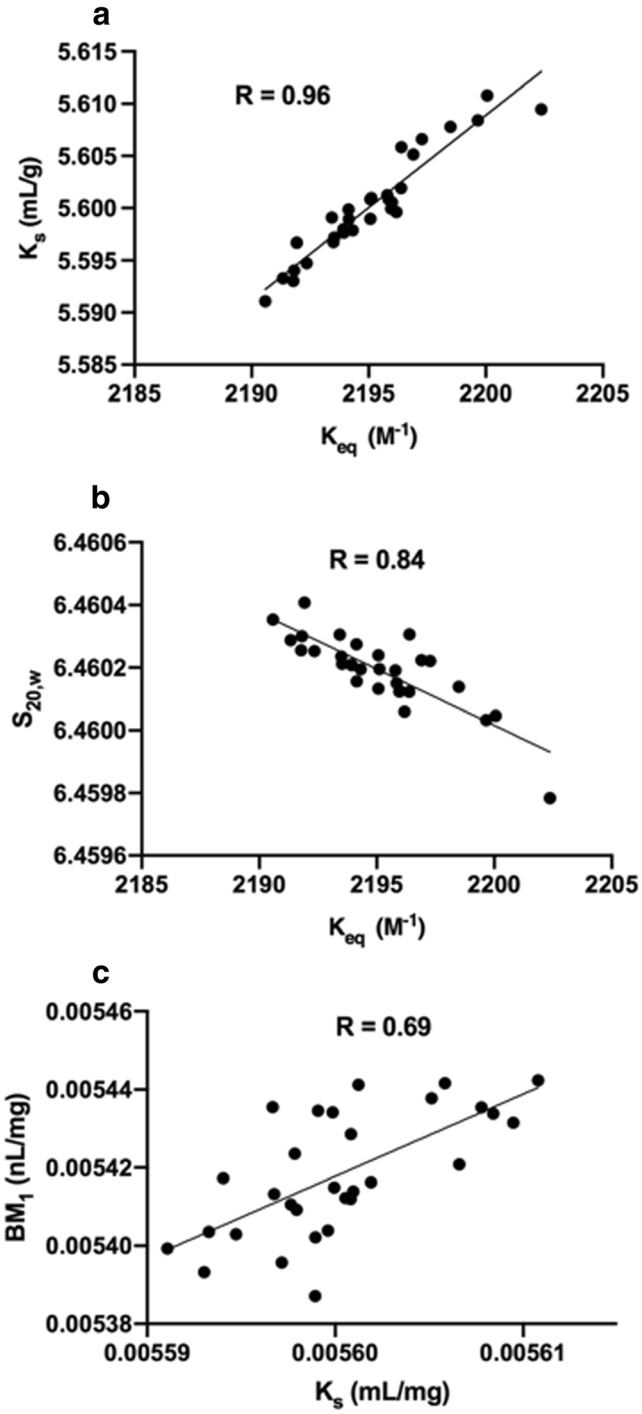

Fig. 7 Selected correlation plots for a weakly interacting, nonideal monomer-dimer system. Sedimentation velocity data were simulated in SEDANAL for mAb concentrations ranging from 0.3 to 13 mg/mL, assuming a monomer-dimer interaction model, and using the following interaction parameters: $s_{20,w}$ = 6.46 S; K_{eq} = 2.195e3 M^{-1}; K_s = 5.6 mL/g; BM_1 = 5.4 mL/g. Upon globally fitting the data, thirty iterations of subsequent fitting were carried using a bootstrap with replacement approach. Selected parameters determined from the bootstrap fits were then plotted against each other to determine the extent of pairwise correlation, R. (**a**) K_{eq} *versus* K_s; (**b**) K_{eq} *versus* $s_{20,w}$; (**c**) K_s *versus* BM_1.

with moderate correlation between seen $S_{20,w}$ and K_{eq} (Fig. 7b), and the least extent between BM_1 and K_s (Fig. 7c). Similar patterns were seen for mAb C at 35°C.

In addition to the above correlations seen for mAb E, for mAb C at 4°C we also observed strong correlation between K_s and the sedimentation coefficient, $s_{20,w}$. This is likely due to the fact that even at the lowest mAb C concentration of 0.3 mg/mL there was still evidence of self-association at this temperature (see Fig. 2a), making it difficult to precisely estimate the monomer sedimentation coefficient. As has been discussed previously, such strong correlation can result in increased imprecision on parameter estimates (40), possibly explaining why the sedimentation coefficient for the monomer is higher than the expected value of ~6.5 S. Alternatively or additionally, it is likely that the assumed relationship of sedimentation coefficients between monomer and higher-order species (based on the $n^{2/3}$ rule) is incorrect, resulting in a skewing of the sedimentation coefficient estimate.

Thermodynamics of mAb-Specific Self-Association

Temperature-dependent self-association studies were carried out to determine enthalpy and entropy terms to identify underlying forces of RSA. In principle, thermodynamic values determined from a van't Hoff plot as shown in Fig. 5 should show no discrepancies relative to a calorimetric determination (41). However, in practice caution is warranted due to experimental limitations (e.g. ability to detect curvature indicative of a heat capacity change). In terms of interpretation of the thermodynamic terms, the classical approach follows that of Ross and Subramanian, in which the signs of the enthalpy and entropy changes are associated with various molecular processes (42). Within this framework, the favorable enthalpy and entropic penalty for mAb C self-association suggests that van der Waals interactions and H-bond formation play a role in RSA. By contrast, the favorable entropy and minimal enthalpy for mAb E self-association implicate electrostatic effects. Taken at face value, the above interpretations both expand and confirm findings of previous studies. For example, previous work on mAb C found that hydrophobic and electrostatics were primary contributors to RSA; however, the authors also identified a thermodynamic signature similar to what was determined here (10). With regard to mAb E, thermodynamic studies are scarcer, although previous work also identified electrostatics as a primary contributor to RSA (19).

The above classical approach has long served as a template for interpreting thermodynamic signatures of macromolecular interactions. However, more recent studies have highlighted limitations, particularly for reactions that are coupled to multiple equilibria (43). in the case of mAb C and E, it is already known that pH, and specific ion- and salt-type, influence RSA (10,19). In the context of linkage thermodynamics, these observations indicate that net proton and ion-binding/release

events are coupled to self-association. Noting that hydrophobic interactions have also been implicated for mAb C RSA (10), water release is also likely coupled. Thus, the thermodynamic signatures determined here almost certainly represent a composite of reactions and are unlikely to be assignable to a single molecular contribution or force.

In summary, this work demonstrates that mAb-specific RSA occurs with unique thermodynamics, suggestive of distinct underlying mechanisms. Although considerably more work will be necessary to elucidate such mechanisms, a more fundamental understanding of mAb-specific RSA may eventually make it possible to engineer primary sequence and/or design new formulations to minimize mAb self-association.

ACKNOWLEDGMENTS AND DISCLOSURES. We are grateful to Jack Correia and Walter Stafford for extensive and insightful discussions, and thank Martin Leon and Cherie Lambert for technical assistance.

SUPPLEMENTARY INFORMATION

The online version contains supplementary material available at https://doi.org/10.1007/s11095-021-02987-0.

Funding

This work was supported by MedImmune, LLC, now a member of AstraZeneca.

DECLARATIONS

Disclosures of Financial Interest The authors declare no financial interest.

REFERENCES

1. Ecker DM, Jones SD, Levine HL. The therapeutic monoclonal antibody market. MAbs. 2015;7(1):9–14. https://doi.org/10.4161/19420862.2015.989042.
2. Goswami S, Wang W, Arakawa T, Ohtake S. Developments and challenges for mAb-based therapeutics. Antibodies. 2013;2(3):452–500.
3. Razinkov VI, Treuheit MJ, Becker GW. Accelerated formulation development of monoclonal antibodies (mAbs) and mAb-based modalities: review of methods and tools. J Biomol Screen. 2015;20(4):468–83. https://doi.org/10.1177/1087057114565593.
4. Jiskoot W, Randolph TW, Volkin DB, Russell Middaugh C, Schöneich C, Winter G, et al. Protein instability and immunogenicity: roadblocks to clinical application of injectable protein delivery systems for sustained release. J Pharm Sci. 2012;101(3):946–54. https://doi.org/10.1002/jps.23018.
5. Shire SJ, Shahrokh Z, Liu J. Challenges in the development of high protein concentration formulations. J Pharm Sci. 2004;93(6):1390–402. https://doi.org/10.1002/jps.20079.
6. Philo JS, Arakawa T. Mechanisms of protein aggregation. Curr Pharm Biotechnol. 2009;10(4):348–51. https://doi.org/10.2174/138920109788488932.
7. Alford JR, Kendrick BS, Carpenter JF, Randolph TW. High concentration formulations of recombinant human interleukin-1 receptor antagonist: II. Aggregation kinetics. J Pharm Sci. 2008;97(8):3005–21. https://doi.org/10.1002/jps.21205.
8. Nishi H, Miyajima M, Nakagami H, Noda M, Uchiyama S, Fukui K. Phase separation of an IgG1 antibody solution under a low ionic strength condition. Pharm Res. 2010;27(7):1348–60. https://doi.org/10.1007/s11095-010-0125-7.
9. Wei JY, Bou-Assaf GM, Houde D, Weiskopf A. Technical decision-making with higher order structure data: detecting reversible concentration-dependent self-Association in a Monoclonal Antibody and a preliminary investigation to eliminate it. J Pharm Sci. 2015;104(11):3984–9. https://doi.org/10.1002/jps.24616.
10. Esfandiary R, Parupudi A, Casas-Finet J, Gadre D, Sathish H. Mechanism of reversible self-association of a monoclonal antibody: role of electrostatic and hydrophobic interactions. J Pharm Sci. 2015;104(2):577–86. https://doi.org/10.1002/jps.24237.
11. Sule SV, Cheung JK, Antochshuk V, Bhalla AS, Narasimhan C, Blaisdell S, et al. Solution pH that minimizes self-association of three monoclonal antibodies is strongly dependent on ionic strength. Mol Pharm. 2012 Apr 2;9(4):744–51. https://doi.org/10.1021/mp200448j Epub 2012 Feb 17.
12. Geoghegan JC, Fleming R, Damschroder M, Bishop SM, Sathish HA, Esfandiary R. Mitigation of reversible self-association and viscosity in a human IgG1 monoclonal antibody by rational, structure-guided Fv engineering. MAbs. 2016;8(5):941–50. https://doi.org/10.1080/19420862.2016.1171444.
13. Hopkins MM, Lambert CL, Bee JS, Parupudi A, Bain DL. Determination of interaction parameters for reversibly self-associating antibodies: a comparative analysis. J Pharm Sci. 2018;107(7):1820–30. https://doi.org/10.1016/j.xphs.2018.03.011.
14. Tanford C. Physical chemistry of macromolecules. New York: Wiley; 1961.
15. Rowe AJ. The concentration dependence of transport processes: a general description applicable to the sedimentation, translational diffusion, and viscosity coefficients of macromolecular solutes. Biopolymers. 1977;16:2595–611. https://doi.org/10.1002/bip.1977.360161202\.
16. Cole JL, Correia JJ, Stafford WF. The use of analytical sedimentation velocity to extract thermodynamic linkage. Biophys Chem. 2011;159(1):120–8. https://doi.org/10.1016/j.bpc.2011.05.014.
17. Correia JJ, Wright RT, Sherwood PJ, Stafford WF. Analysis of nonideality: insights from high concentration simulations of sedimentation velocity data. Eur Biophys J. 2020 Dec;49(8):687–700. https://doi.org/10.1007/s00249-020-01474-5. Epub 2020 Nov 6.
18. Esfandiary R, Hayes DB, Parupudi A, Casas-Finet J, Bai S, Samra HS, et al. A systematic multitechnique approach for detection and characterization of reversible self-association during formulation development of therapeutic antibodies. J Pharm Sci. 2013;102(9):3089–99. https://doi.org/10.1002/jps.23654.
19. Arora J, Hu Y, Esfandiary R, et al. Charge-mediated Fab-Fc interactions in an IgG1 antibody induce reversible self-association, cluster formation, and elevated viscosity. MAbs. 8(8):1561–74. https://doi.org/10.1080/19420862.2016.1222342.
20. Hu Y, Arora J, Joshi SB, Esfandiary R, Middaugh CR, Weis DD, et al. Characterization of excipient effects on reversible self-association, backbone flexibility, and solution properties of an IgG1 monoclonal antibody at high concentrations: part 1. J Pharm Sci. 2020;109(1):340–52. https://doi.org/10.1016/j.xphs.2019.06.005.
21. Hu Y, Toth RT 4th, Joshi SB, et al. Characterization of excipient effects on reversible self-association, backbone flexibility, and

solution properties of an IgG1 monoclonal antibody at high concentrations: part 2. J Pharm Sci. 2020;109(1):353–63. https://doi.org/10.1016/j.xphs.2019.06.001.

22. Arora J, Hickey JM, Majumdar R, Esfandiary R, Bishop SM, Samra HS, et al. Hydrogen exchange mass spectrometry reveals protein interfaces and distant dynamic coupling effects during the reversible self-association of an IgG1 monoclonal antibody. MAbs. 2015;7(3):525–39. https://doi.org/10.1080/19420862.2015.1029217.
23. Hayes D, Laue T, Philo J. Program SEDNTERP: Sedimentation interpretation program. Durham, NH: University of New Hampshire;1995, www.jphilo.mailway.com/download.htm#sednterp
24. Stafford WF 3rd. Boundary analysis in sedimentation transport experiments: a procedure for obtaining sedimentation coefficient distributions using the time derivative of the concentration profile. Anal Biochem. 1992;203(2):295–301. https://doi.org/10.1016/0003-2697(92)90316-y.
25. Philo JS. Improved methods for fitting sedimentation coefficient distributions derived by time-derivative techniques. Anal Biochem. 2006;354(2):238–46. https://doi.org/10.1016/j.ab.2006.04.053.
26. Stafford WF, Sherwood PJ. Analysis of heterologous interacting systems by sedimentation velocity: curve fitting algorithms for estimation of sedimentation coefficients, equilibrium and kinetic constants. Biophys Chem. 2004;108(1–3):231–43. https://doi.org/10.1016/j.bpc.2003.10.028.
27. Claverie JM, Dreux H, Cohen R. Sedimentation of generalized systems of interacting particles. I. Solution of systems of complete Lamm equations. Biopolymers. 1975;14(8):1685–700. https://doi.org/10.1002/bip.1975.360140811.
28. Claverie JM. Sedimentation of generalized systems of interacting particles. III. Concentration-dependent sedimentation and extension to other transport methods. Biopolymers. 1976;15(5):843–57. https://doi.org/10.1002/bip.1976.360150504.
29. Sorret LL, DeWinter MA, Schwartz DK, Randolph TW. Challenges in predicting protein-protein interactions from measurements of molecular diffusivity. Biophys J. 2016 Nov 1;111(9):1831–1842. https://doi.org/10.1016/j.bpj.2016.09.018.
30. Correia JJ. Analysis of weight average sedimentation velocity data. Methods Enzymol. 2000;321:81–100. https://doi.org/10.1016/s0076-6879(00)21188-9.
31. Sontag CA, Stafford WF, Correia JJ. A comparison of weight average and direct boundary fitting of sedimentation velocity data for indefinite polymerizing systems. Biophys Chem. 2004;108(1–3):215–30. https://doi.org/10.1016/j.bpc.2003.10.029.
32. Correia JJ, Stafford WF. Extracting equilibrium constants from kinetically limited reacting systems. Methods Enzymol. 2009;455:419–46. https://doi.org/10.1016/S0076-6879(08)04215-8.
33. Creeth JM, Knight CG. On the estimation of the shape of macromolecules from sedimentation and viscosity measurements. Biochim Biophys Acta. 1965;102(2):549–58. https://doi.org/10.1016/0926-6585(65)90145-7.
34. Yang D, Correia JJ, Stafford WF III, et al. Weak IgG self- and hetero-association characterized by fluorescence analytical ultracentrifugation. Protein Sci. 2018;27(7):1334–48. https://doi.org/10.1002/pro.3422.
35. Wright RT, Hayes DB, Stafford WF, Sherwood PJ, Correia JJ. Characterization of therapeutic antibodies in the presence of human serum proteins by AU-FDS analytical ultracentrifugation. Anal Biochem. 2018 Jun;550:72–83. https://doi.org/10.1016/j.ab.2018.04.002.
36. Diebolder CA, Beurskens FJ, de Jong RN, Koning RI, Strumane K, Lindorfer MA, et al. Complement is activated by IgG hexamers assembled at the cell surface. Science. 2014;343(6176):1260–3. https://doi.org/10.1126/science.1248943.
37. de la Torre JG, Echenique Gdel R, Ortega A. Improved calculation of rotational diffusion and intrinsic viscosity of bead models for macromolecules and nanoparticles. J Phys Chem B. 2007;111(5):955–61. https://doi.org/10.1021/jp0647941.
38. Lin J, Lucius AL. Examination of the dynamic assembly equilibrium for E. coli ClpB. Proteins. 2015;83(11):2008–24. https://doi.org/10.1002/prot.24914.
39. Philo JS. Characterizing the aggregation and conformation of protein therapeutics. American Biotechnology Laboratory. 2003;21(11):22–6.
40. Johnson ML. Parameter correlations while curve fitting. Methods Enzymol. 2000;321:424–46. https://doi.org/10.1016/s0076-6879(00)21207-x.
41. Horn JR, Russell D, Lewis EA, Murphy KP. Van't Hoff and calorimetric enthalpies from isothermal titration calorimetry: are there significant discrepancies? Biochemistry. 2001;40(6):1774–8. https://doi.org/10.1021/bi002408e.
42. Ross PD, Subramanian S. Thermodynamics of protein association reactions: forces contributing to stability. Biochemistry. 1981;20(11):3096–102. https://doi.org/10.1021/bi00514a017.
43. Winzor DJ, Jackson CM. Interpretation of the temperature dependence of equilibrium and rate constants. J Mol Recognit. 2006;19(5):389–407. https://doi.org/10.1002/jmr.799.